

An Integrated Approach to Modeling and Mitigating SOFC Failure
(Agreement No. DE-AC26-02NT41571)

Monthly Project Highlight Report

for the period of

August 1, 2003 – August 30, 2003

to

Travis R. Shultz
National Energy Technology Laboratory

From

PI: Jianmin Qu,
Co-PIs: Andrei Fedorov and Comas Haynes

School of Mechanical Engineering
Georgia Institute of Technology
801 Ferst Drive, N.W.
Atlanta, Georgia 30332-0405
Phone: 404-894-5687
FAX: 404-894-0186
E-Mail: jianmin.qu@me.gatech.edu

August 30, 2003

Agreement No.: DE-AC26-02NT41571

Reporting Period: – August 1, 2003 – August 30, 2003

Summary of Activities

Major activities of this month include

- Developed a domain integration formulation to evaluate crack tip parameters for fracture analysis.
- Conducted thermal-fluid simulation on co-flow, counter-flow and cross-flow model cells with multiple channel resolution.
- Linked Fluent results with FEA (Ansys) tool by successfully transferring the temperature field results of the different SOFC flow configuration models to a corresponding stress analysis model.

Technical Highlights

Task 1: Fracture Mechanics Modeling

1.3 Identify and Quantify Crack Path Selection and Crack Propagation

Domain Integral Formulation

The domain integral formulation is often used to calculate fracture parameters in three-dimensional finite element programs. The method's significance is based on the fact that for an isotropic material experiencing elastic deformation the domain integral equals the energy release rate. Recall that the energy release rate (G) is a measure of the energy available for crack growth to occur. If the energy release rate of a system is greater than the fracture toughness (G_c), an intrinsic material property, then the crack will grow.

This method of analysis is preferred for several reasons. Firstly, it is based on the energy changes of the system, and not strictly on calculation of stress or strain fields surrounding the crack tip. This means that the difficult problem of accurately meshing the crack tip is greatly simplified. Another important aspect of the domain integral is that it allows the calculation of a pointwise energy release rate along the crack edge allowing observation of fracture behavior at different locations on the crack tip.

The volumetric form of the domain integral is shown in equation 1.1. The internal components of the integral represent the energy momentum tensor (\mathbf{P}) multiplied by the change in virtual crack growth. Equation 1.1 assumes the absence of crack face tractions.

$$\begin{aligned}\bar{G} = \bar{J} &= -\int_V tr[\mathbf{P} \cdot \bar{\nabla} \mathbf{q}] dV \\ \mathbf{P} &= W\mathbf{I} - (\bar{\nabla} \mathbf{u} \cdot \boldsymbol{\sigma})\end{aligned}\tag{1.1}$$

The strain energy density (W) of the system is a scalar quantity that measures the total work per unit volume of the system. The second part of (1.1) consists of the strain

and stress fields surrounding the crack, where $\bar{\nabla} \mathbf{u}$ is the derivative of the displacements and $\boldsymbol{\sigma}$ is the stress tensor.

The test function \mathbf{q} is dependant on the location within the volume and is equivalent to the virtual crack growth. In its simplest form it is the crack extension normal to the crack plane. As shown in Figure 1.1, when a crack undergoes growth at a point S, a continuous function can be considered to represent the growth for some arc length on the crack tip.

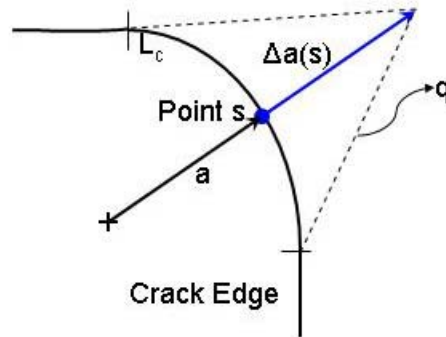


Figure 1.1: Continuous function q on crack tip

The pointwise value of the energy release rate is found with the assumption that for a small chord length (L_c) the energy release rate represents an average value within the volume. Therefore area division results in the value at point S as shown in equation 1.2. The units of the pointwise value of the energy release rate ($G(s)$) are energy over area, while \bar{G} has dimensions energy per length.

$$G(s) = \frac{\bar{G}}{\int_{L_c} \Delta a(s) ds} \quad (1.2)$$

Finite Element Implementation

Since most commercial softwares have limited or no domain integral capabilities it is often calculated separately during postprocessing. For the purposes of this study the finite element programs were performed using the software ANSYS 7.0 with the post processing performed using the commercial programming language Matlab 6.5. Development of the postprocessing procedure was based on the procedures described from references from Li (Engineering Fracture Mechanics, 1985) and Gosz (Int. J. Solids Structures, 1998). Figure 1.2 is a flow chart representing the steps taken during postprocessing.

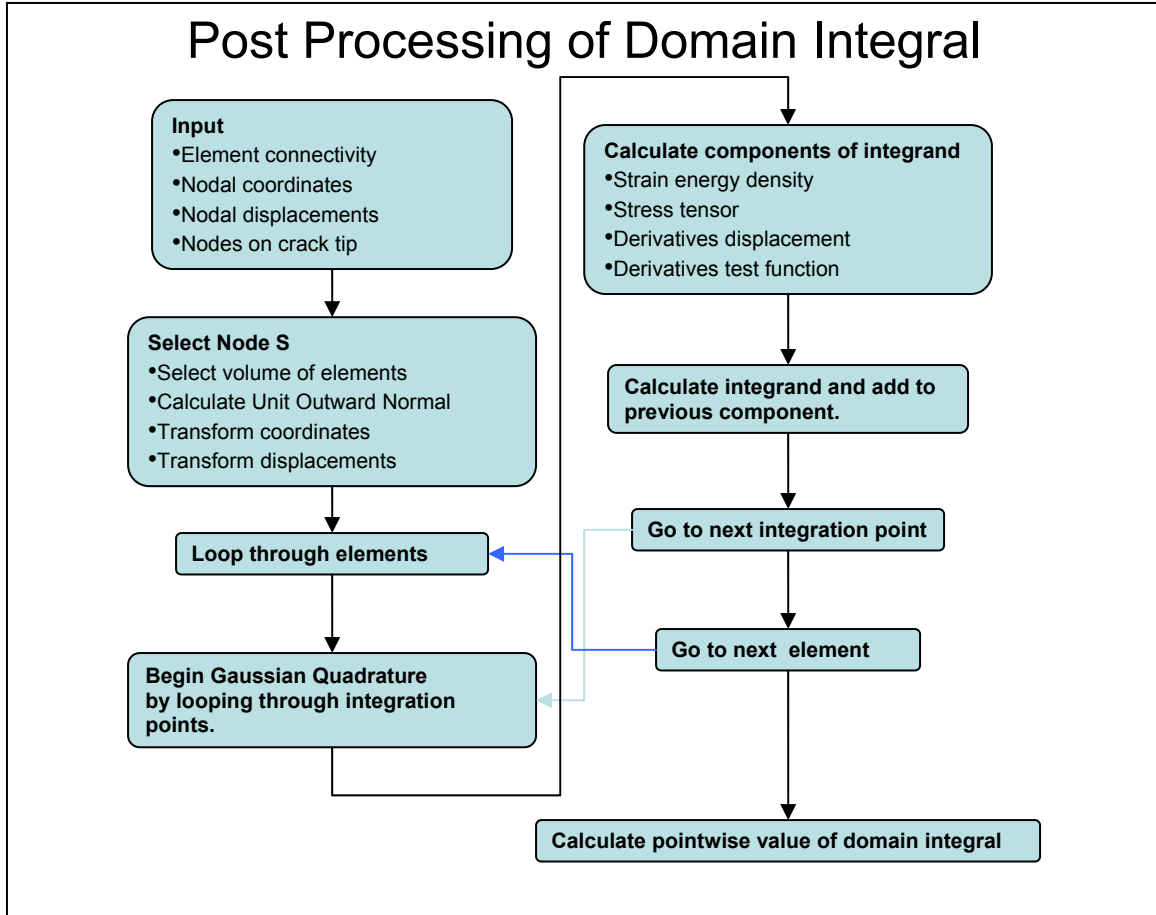


Figure 1.2: Flow Chart Postprocessing Steps

The following is a brief description on the methods to calculate the internal components of the domain integral. Several basic concepts and constants concerning calculation of stress and strain from finite element methods are included in Appendix A. Gaussian quadrature is also briefly explained.

Determination of the strain energy density of an element can be calculated by integrating the stress tensor multiplied by strain over the volume of an element.

$$W = \int_0^{\epsilon} \sigma d\epsilon \quad (1.4)$$

For the purposes of numerical analysis it is simpler if the strain energy is developed separately from the volume. Using Gaussian quadrature and Hooke's law the strain energy can be written as:

$$U^{(e)} = \int_V \frac{1}{2} \boldsymbol{\epsilon}^T \mathbf{E} \boldsymbol{\epsilon} dV = \frac{1}{2} \mathbf{u}^T \left(\int_V \frac{1}{2} \mathbf{B}^T \mathbf{E} \mathbf{B} dV \right) \mathbf{u} \quad (1.5)$$

$$U^{(e)} = \frac{1}{2} \mathbf{u}^T \left(\int_{-1}^1 \int_{-1}^1 \int_{-1}^1 (\mathbf{B}^T \mathbf{E} \mathbf{B}) \det J \, dr \, ds \, dt \right) \mathbf{u} \quad (1.6)$$

$$U^{(e)} = \frac{1}{2} \mathbf{u}^T \left(\sum_{k=1}^2 \sum_{l=1}^2 \sum_{m=1}^2 (\mathbf{F}(r,s,t))_{ij} \det J w_k w_l w_m \right) \mathbf{u}$$

where $F_{ij} = (\mathbf{B}^T \mathbf{E} \mathbf{B})_{ij}$ ($i, j = 1, 2, \dots, \text{node}$) and J is the Jacobian.

The strain energy can then be divided by the element volume to calculate the strain energy density (1.4).

$$W^{(e)} = \frac{U^{(e)}}{V^{(e)}} \quad (1.7)$$

$$V^{(e)} = \sum_{k=1}^2 \sum_{l=1}^2 \sum_{m=1}^2 \det J w_k w_l w_m$$

The second part of the momentum tensor looks at the stress and strain fields within the volume. Using the chain rule the derivatives of the displacements can be calculated by equation (1.5), while the stress tensor is in 3x3 symmetric matrix form and can be calculated from steps in Appendix A.

$$\frac{\partial u_i^{(e)}}{\partial x_j} = \sum_{l=1}^8 \sum_{j=1}^3 \frac{\partial N_l}{\partial r_j} \frac{\partial r_j}{\partial x_j} u_{il} \quad (1.8)$$

Lastly the test function q needs to be fully defined. If the node of interest (S), is taken to be the new origin and the nodal coordinates and transformations are translated as shown in Figure 1.3 the definition of q is simplified. The unit outward normal to the crack tip represents the crack growth and nodes on the outer boundary are zero.

$$Q_{ai} = \begin{cases} [1 & 0 & 0] & \text{for nodes on } x' \\ 0 & \text{on outer boundary} \end{cases} \quad (1.9)$$

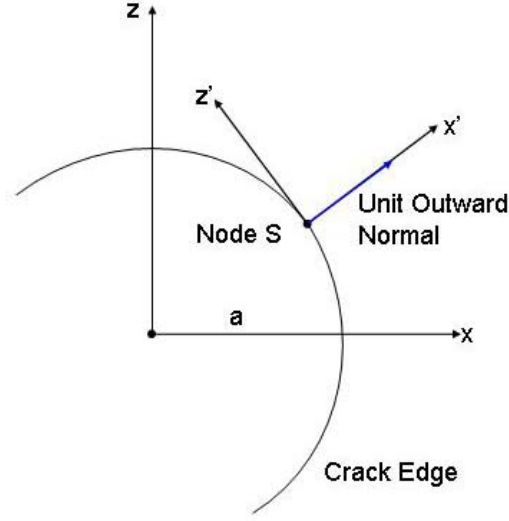


Figure 1.3: Transformation to new coordinate system

The test function is also an isoparametric function which means the derivatives can be taken in the same fashion as that of the strains.

$$\frac{\partial q_i^{(e)}}{\partial x_j} = \sum_{l=1}^8 \sum_{j=1}^3 \frac{\partial N_l}{\partial r_j} \frac{\partial r_j}{\partial x_j} Q_{il} \quad (1.10)$$

It is now possible to calculate the average domain integral and the energy release rate at node S.

$$\bar{G} = -\sum_{e \in V} \left\{ \sum_{k=1}^2 \sum_{l=1}^2 \sum_{m=1}^2 \left(\text{tr} \left[\mathbb{M} \mathbb{I} - \bar{\nabla} u \square \sigma \right] \bar{\nabla} q \right)_{ij} \det J w_k w_l w_m \right\} \quad \text{where } (i, j = 1, 2, \dots, \text{node}) \quad (1.11)$$

Before calculating the pointwise value the chord lengths between nodes S and the nodes S+1 and S-1 on the crack tip needs to be defined as L_1 and L_2 . If the values are known then:

$$G(s) = \frac{2\bar{G}}{L_1 + L_2} \quad (1.12)$$

For this method of calculation the meshing and volume selection for the domain integral have some minor requirements. A mapped mesh was used to insure that selected nodes were always normal to the crack plane. Secondly, while the size of the volume is flexible perpendicular to the crack and normal to the crack only one row of elements can be included on either side of node S. This is necessary for more accurate calculation of the pointwise value.

Finite Element Information and Verification Model:

A fixed displacement model was created to verify the accuracy of the postprocessing step of the domain integral. The local/global process used previously was also included in the analysis. The top boundary of the global model was loaded at a constant displacement of .01 mm giving a constant tensile stress of 1627MPa throughout the model. The material properties were 96GPa for the modulus of elasticity and a Poisson's ratio of 0.3.

Fracture was added to the analysis by using a cylindrical local model containing a penny shaped crack at its center. The local model was placed at the center of the global model. The crack radius (a) was set to .001mm. As discussed in past reports the local model is analyzed by using the displacements from the global model as boundary conditions for the exterior of the local mesh. The local model width was .08mm.

The model consisted of 8 node brick elements assembled in a cylindrical mapped mesh. Elements along the crack tip were set equal to $e=a/10$. A row of 5 elements extending vertically from the crack plane were also set to this ratio. On the crack plane the elements immediately outside the penny shaped crack were set to $e/2$. The default element size for elements outside the crack region was approximately $5e$. In all, 36864 elements were used to construct the model with dimensions as shown in Figure 1.4.

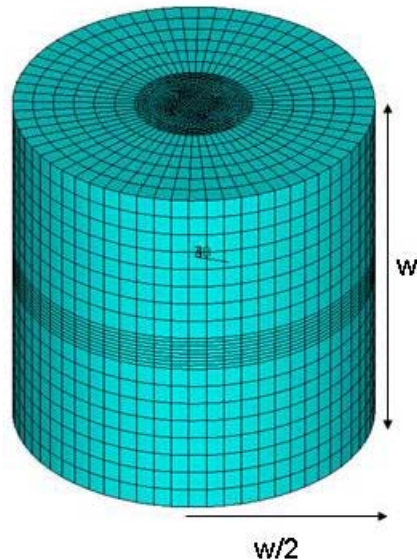


Figure 1.4: Mesh of local model

This analysis was chosen because it simulates behavior of a crack in an infinite body, which has a known solution. Another important aspect is that the energy release rate is constant around the edges of the crack tip and can be calculated with equation (1.13). For the parameters given the energy release rate should equal 0.35 kJ/m^2 .

$$G = \frac{K_I^2}{E} = \frac{1}{E} \left(\frac{2}{\pi} \sigma \sqrt{\pi a} \right)^2 \quad (1.13)$$

A small section of elements was taken from the crack tip and analyzed using the domain integral formulation. Figure 1.5 shows the elements selected and the stress behavior along the crack tip, while Table 1.1 lists the results of the nodes along the crack edge.

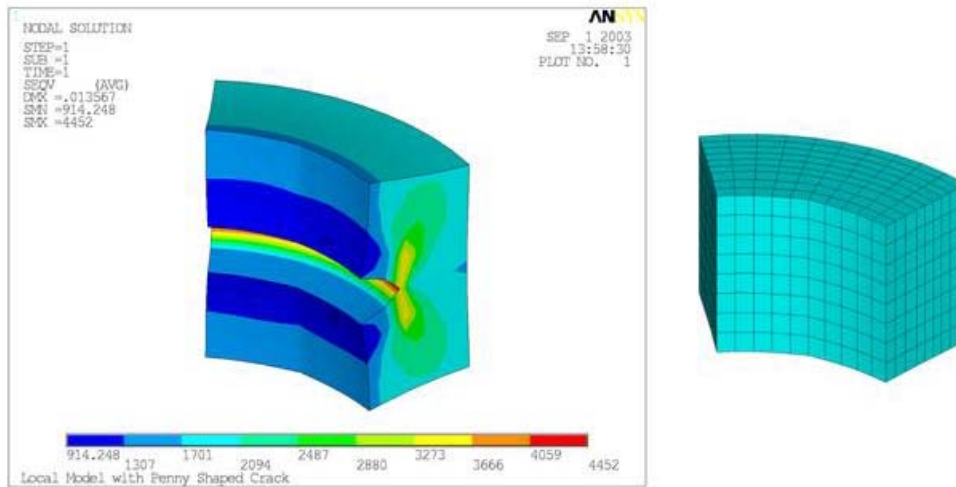


Figure 1.5: Von Mises Stresses of penny shaped crack in an infinite body (deformation 10:1 scale) and related crack tip mesh.

Table 1.1: Pointwise Values of Domain Integral

Node	1	2	3	4	5	6	7	8	9	Average	Actual
G(s)—kJ/m²	.36	.35	.36	.38	.47	.38	.32	.38	.41	.38	.35

The values shown in Table 1.1 represent the domain integral calculations for nine consecutive volumes along the crack tip. While some of these values are fairly high they are still consistent. The exceptionally high value at node 5 is most likely due to an irregularity in the mesh due to the requirements of mapped meshing. The mesh used for the local model was selected for efficiency and tested with an Ansys 7.0 macro of the line integral form of the domain integral. It calculated a value of 0.41 kJ/m². This suggests improvements could be made on the mesh, but also shows the greater accuracy of the domain integral.

There are several ways to reduce the error occurring in the domain integral formulation. A simple method would be to increase the volume analyzed so crack tip singularities do not effect the calculation. Also refinement of the mesh could take place either by decreasing element size or increasing element order, for instance switching to a 20 node brick element.

Several steps could also be taken during postprocessing. Errors often occur in calculation of displacements and stresses for eight node quadrilateral elements. Ansys does not have the capability to output the extra displacements necessary for extra shape

functions to reduce these errors, therefore steps would need to be taken to switch to a 20 node element. Another possible solution is to increase the order of quadrature to a 3x3x3. However, the domain integral has been shown to converge around the nodes on a crack tip for any volume.

Planer SOFC Applications

The domain integral was quickly applied to the planer fuel cell to highlight possibilities for analysis. Initially the global model was constructed using a 20 node brick element as described in Table 1.2. Periodic boundary conditions were applied which means the final stress behavior can be considered symmetric around the x and y axis. A total of 420 elements were used.

Table 1.2 Mesh Parameters

PEN Location	Size Ratio	Actual Size - μm (2mm x 1.5mm base)
Length (x-dir)	Length/20	200
Anode (y-dir)	Anode height /8	62.5
Electrolyte (y-dir)	Electrolyte Height/2	7.5
Cathode (y-dir)	Cathode Height/4	18.75
Width (z-dir)	Length/20	150

Table 1.3 Properties used in Finite Element Analysis

Materials	Young's Modulus (GPa)	Poisson's Ratio	CTE (10-6/ $^{\circ}\text{C}$)	Layer Thickness (mm)
Cathode (LSM+YSZ)	96	0.3	10.56	0.075
Electrolyte (YSZ)	200	0.3	10.56	0.015
Anode (Ni+YSZ)	96	0.3	12.22	.5

The model was considered to experience a temperature increase of 1000 degrees causing thermal stresses due to thermal expansion. The following figure shows the Von Misses stress behavior within the volume. The deformation of the figure was increased by a factor of 20 to help illustrate the stress behavior.

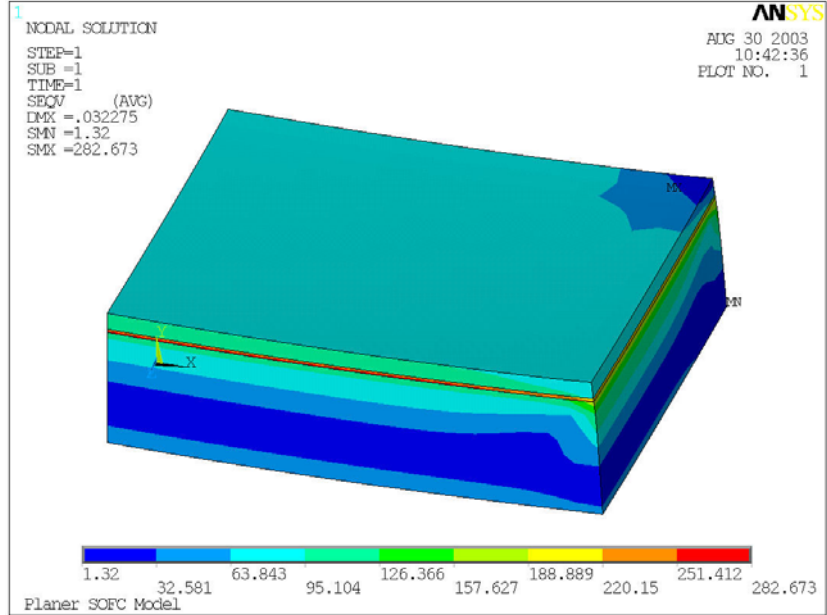


Figure 1.6: Von Misses Stresses of a Planer Fuel Cell

The local model used on the planer fuel cell is exactly the same as that used in the verification model. The center of the model was set at $(.5,.4,0)$. This places the model in the center of the anode with the crack .06mm from the electrolyte. The only difference in analysis is the addition of a temperature field from the global model on all the nodes of the local model. The following figure shows the Von Misses stresses for an element selection around the crack tip.

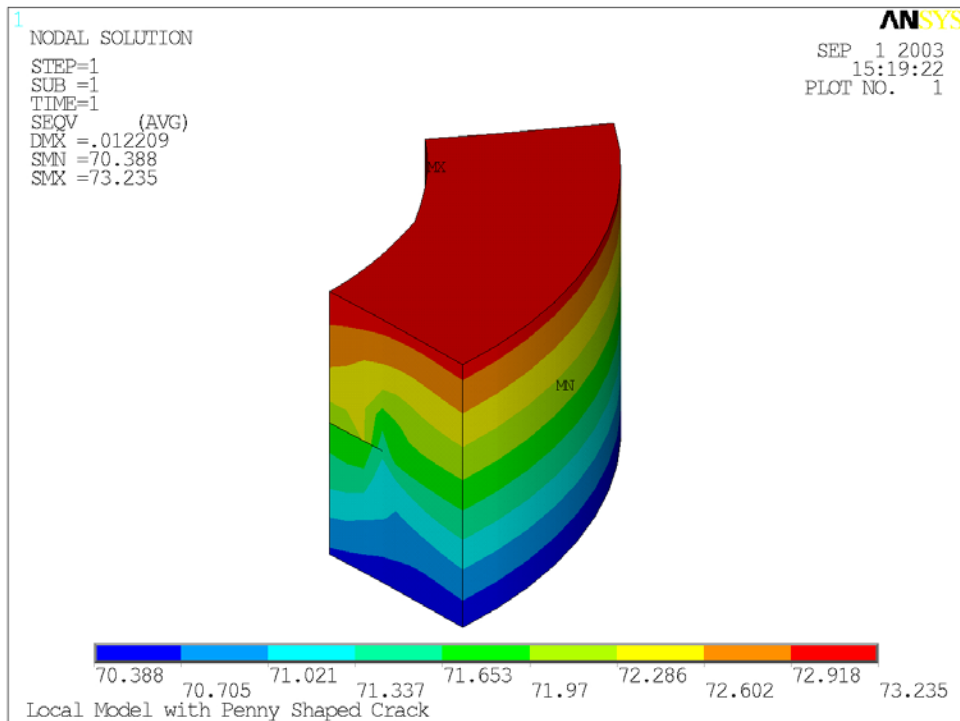


Figure 1.7: Von Misses Stresses around crack tip

Table 1.4: Domain Integral for SOFC (extends 30° either side z=0 axis)

Node	1	2	3	4	5	6	7	8	9	Average	Actual
G(s)—kJ/m²	.21	.20	.20	.20	.25	.25	.20	.20	.21	.213	--

Conclusion

This report has formulated the steps necessary to fully study three-dimensional fracture in fuel cells. The global/local model technique will reduce processing time and allow for greater variability of analyses. The importance of the domain integral technique is highlighted by Figures 1.6 and 1.7 and even in its roughest form the variation along the crack tip can be studied. As the temperature fields grow more complex within the fuel cell so will the stress fields. It is of utmost importance to be able to study the energy release rate at any point on a crack edge.

Task 2: Electrochemical Modeling

This month's electrochemical modeling activities were primarily comprised of continued efforts toward including direct internal reformation (DIR) effects within the solid oxide fuel cell models and interfacing extensively with the SECA national labs/vertical teams regarding the status of their simulation efforts.

Regarding the DIR simulation, previous attempts at modeling extremely high methane concentrations within the reformat (e.g., 40%) were unsuccessful from a convergence standpoint; the problem is understood to stem from an inability to obtain prescribed fuel utilizations. At lower methane concentrations (e.g., 5%), however, which are more indicative of expected reformat streams; solutions are being achieved and compared to “inert hydrocarbon” scenarios with the same reformat composition (results to be included within in next month’s monthly/final report).

Regarding heightened interactions with SECA partners, August concluded with a simulation and modeling training session at PNNL. SECA modeling groups, and those interested, from PNNL, NETL, SECA vertical teams and academia convened to understand the state of software development within the SECA labs’ infrastructure and prepare a roadmap for future direction (i.e., into Phase II development). The implementation/results of various models on various platforms including spreadsheets (Excel), CFD (STAR-CD, FLUENT), FEA (MARC) and combinations thereof were illustrated as a prelude to a near-term “toolkit” for the vertical teams to use. The September SECA review will foster greater software collaborative discussions leading into Phase II.

Tasks 3: Thermal-Fluid Modeling

The “planar bi-polar” geometry of SOFC includes the “co-flow” and “counter flow” cases where the air and gas channels are parallel, and the “cross-flow” case where the channels are perpendicular. The later case is preferred by industry because of the simplicity involved in manifolding. In order to analyze the thermo-mechanical failure modes in commonly found SOFCs, generic unit cells in cross-, co-, and counter-flow configurations were studied for benchmark analysis of temperature and electrical current

distribution. The unit cell is constructed of a positive electrode-electrolyte-negative electrode (PEN) and an interconnect plate stacked together (Fig. 3.1). The co- and counter-flow cases were captured through a simplified unit cell of 5 cm length with bipolar channels. The periodicity in the fuel cell configurations was employed to reduce the model analyses to a single flow channel. In the cross-flow model, a 5 cm x 5 cm unit cell (Fig. 3.2) with 11 channels for air and fuel flow was modeled. A fine mesh was employed near the channel walls to account for the boundary layer development.

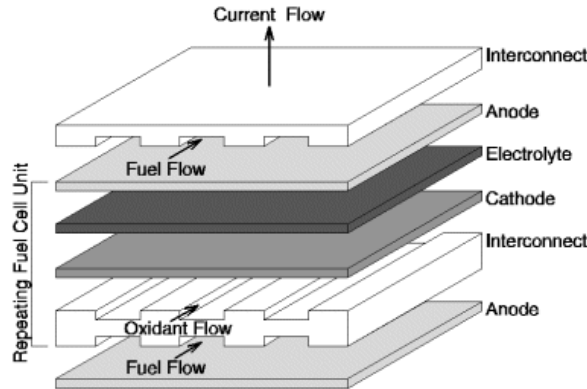


Figure 3.1: Schematic of a co-flow configuration fuel cell unit

Constant temperature, velocity and mixture composition were imposed at the inflow boundaries for the fuel and air. The flow rates were determined by the current demand and computed using the Faraday's law for an 85 % utilization of 78 % H_2 and 22 % H_2O molar composition fuel stream. Conditions for the benchmark simulations were chosen to achieve an average current density of 150 mA/cm^2 and 450 mA/cm^2 with the air stream delivered at 650 K and the fuel stream supplied at 800 K.

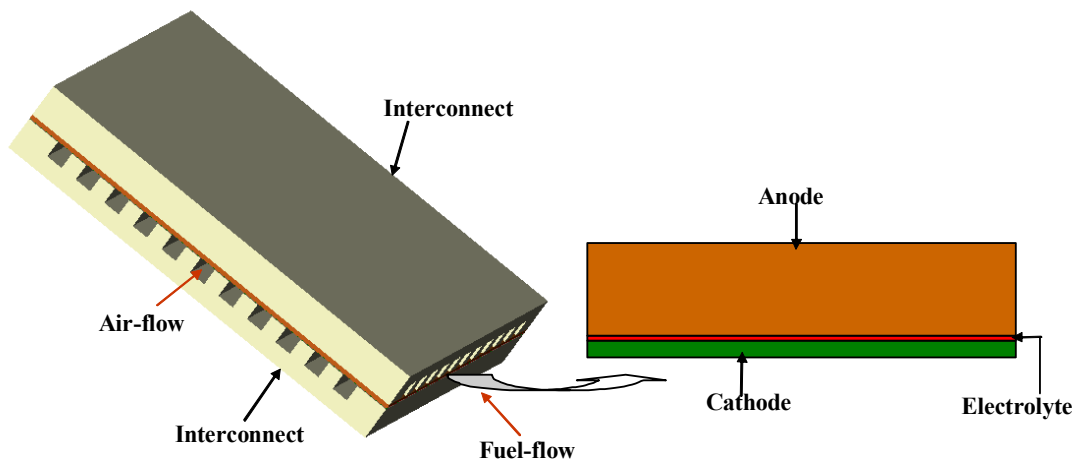


Figure 3.2: Schematic sketch of the cross-flow planar fuel cell model with an expanded view of PEN structure.

Results

Figure 3.3 plots the temperature variation along the anode-electrolyte interface for the co-flow and counter-flow cases. Figure 3.2 shows the temperature distribution along

the anode-electrolyte interface for the cross-flow configuration unit cell, wherein the arrangement of the fuel and air manifolds results in non-uniform temperature distributions with steep temperature gradients across the fuel cell. In each case, the temperature increased along the airflow direction, reaching a maximum near the air exit. Of the three flow configurations tested, the counter-flow case had the most uniform temperature distribution and smallest temperature difference along the electrode-electrolyte interface for higher current densities. This is in agreement with the data reported in literature (Ferguson et al., 1996).

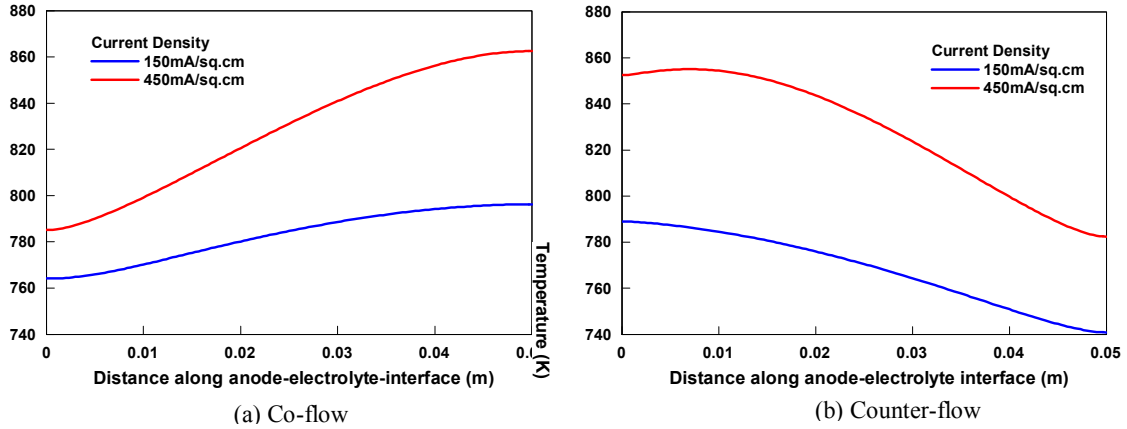


Figure 3.3: Plot of variation of temperature along the centerline passing through the anode-electrolyte interface for (a) co-flow and (b) counter-flow configurations. Counter-flow arrangement results in more uniform temperature distribution.

Table 3.1 summarizes the results from the three flow configurations studied. Of the three flow configurations tested, the average PEN temperature and the temperature variation per unit length of the PEN were found to be maximum for the cross-flow fuel cell configuration at higher current densities.

Table 3.1: Comparison of results from different flow configurations

Current Density	Co-flow	Counter-flow	Cross-flow
150 mA/cm²			
Cell Voltage (V)	0.966	0.971	0.963
T_{avg} (K)	782.6	768.2	786.0
450 mA/cm²			
Cell Voltage (V)	0.743	0.745	0.733
T_{avg} (K)	828.2	826.0	845.5

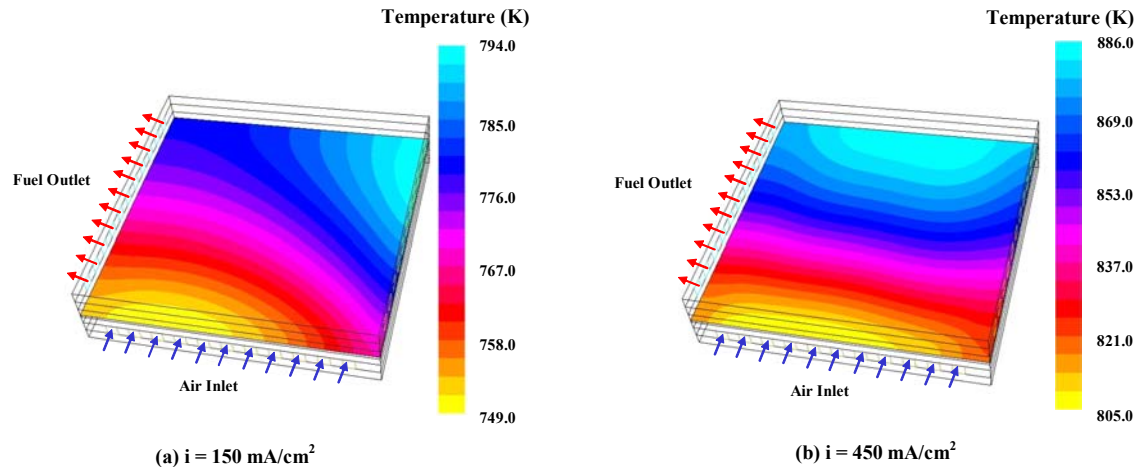


Figure 3.4: Temperature contours for the cross-flow configuration for two different current densities, namely (a) 150 mA/cm² and (b) 450 mA/cm² along the anode-electrolyte interface.

The cross-flow case, due to its non-uniform temperature distribution and large temperature gradients, is highly susceptible to thermomechanical failure. The temperature field from the Fluent simulation of the cross-flow fuel cell arrangement was transferred to a corresponding model in Ansys for further studies on thermo-mechanical stress and reliability analysis.

References

Ferguson, J.R., Fiard, J.M., and Herbin, R., “Three-Dimensional Numerical Simulation for various Geometries of Solid Oxide Fuel Cells” *Journal of Power Sources*, vol. 58, pp. 109-122, 1996.

Completed Tasks

Tasks 1.1, 1.2, 1.3, 1.4, 2.2, 2.3, 3.1, 3.2, 3.3, 3.4 and 4.2 are complete, all others are on going.

Key Milestone Update

Tasks	Status	Remarks
1.1 Obtain fracture mechanics parameters for cohesive, interfacial and impinging cracks.	100% complete	
1.2 Model spalling phenomenon and thermal expansion induced stress during thermal transients and shock.	100% complete	
1.3 Identify and quantify crack path selection and crack propagation.	100% complete	
1.4 Implement temperature gradient as driving force for cracking. The Recipient	100% complete	

shall investigate the individual and combined influences of electrochemical and mechanical load stress, as well as temperature gradients on crack initiation and propagation. The Recipient shall review and utilize/adapt, where appropriate, existing, available fracture mechanics models in order to advance the state-of-the-art.		
1.5 Evaluate and validate the accuracy of developed fracture mechanics models using either experimental data or modeling results from PNNL/NETL/ORNL or other SECA members.	90% complete	
2.1 Utilize/adapt existing electrochemical models, and develop enhancements necessary to achieve the project objectives and to advance the state-of-the-art.	90% complete	
2.2 Models Extension to include porous electrode phenomena enhancements beyond the current state-of-the-art.	100% complete	
2.3 Evaluate and validate the accuracy of developed electrochemical models and enhancements using either experimental data or modeling results from PNNL/NETL/ORNL or other SECA members.	100% complete	
3.1 Formulation of 2-D and 3-D models for combined advection, conduction, and radiation heat and mass transfer in the porous electrodes.	100% complete	
3.2 Formulation of an approach for calculation of effective transport, thermophysical and radiative properties for the porous electrodes.	100% complete	I
3.3 Formulation of coupled heat/mass transfer and electrochemistry model on the "unit-cell" level. The Recipient shall account for boundary effects, such as oxidant and fuel flow field channels, electrical interconnects and seals.	100% complete	.
3.4 Review, select, and develop solution algorithms for numerical solution.	100% complete	
3.5 Evaluate and validate the accuracy of developed thermal models, algorithms and enhancements using either experimental	90% complete	

data or modeling results from PNNL/NETL/ORNL or other SECA members.		
4.1 Review the implementation strategy of developed modeling modules within the PNNL/NETL simulation platform.	90% complete	
4.2 Assess and identify areas within the PNNL/NETL simulation platforms where improvements will advance the state-of-the-art and contribute to the overall SECA Modeling and Simulation Program.	100% complete	

Discussion Topics

A licensing contract has been signed between GT and MSC. The Marc software should be installed soon. Per previous discussions, it may become necessary in the near future to obtain some computational time on the new computer purchased recently by PNNL.

Significant Accomplishments

- Conducted thermal-fluid simulation on co-flow, counter-flow and cross-flow multichannel SOFC using Fluent and transferred the temperature fields to the FEA Stress Analysis tool (ANSYS) to perform a corresponding stress analysis model.
- Developed a domain integration formulation to evaluate crack tip parameters for fracture analysis.

Science & Technology Transfer

None to report

Presentations & Publications

None to report

Site Visits

None to report

Travel

C. Haynes attended SECA Core Phase I Simulation and Modeling Training at PNNL..

APPENDIX A

Finite Element Methods

Before the components of the domain integral can be calculated several basic constants and formula's concerning finite element need to be defined. The first one of these is the concept of isoparametric functions, in which the nodal quantities can be mapped onto an element if the shape functions are known.

$$\phi^{(e)} = \sum_{i=1}^{node} N_i \Phi_i \quad (A.1)$$

The shape functions for an 8 node quadrilateral element are as follows:

$$\begin{aligned} N_i &= \frac{1}{8} ((1+rr_i)(1+ss_i)(1+tt_i)) \\ \frac{dN_i}{dr} &= \frac{1}{8} (r_i(1+ss_i)(1+tt_i)) \\ \frac{dN_i}{ds} &= \frac{1}{8} (s_i(1+rr_i)(1+tt_i)) \\ \frac{dN_i}{dt} &= \frac{1}{8} (t_i(1+ss_i)(1+rr_i)) \end{aligned} \quad (A.2)$$

where i is the node number, (r, s, t) is the integration point of interest, and (r_i, s_i, t_i) is the corresponding natural coordinates of the node i .

Now the strains and stresses within an element need to be related to the nodal coordinates and displacements collected from the finite element program:

$$\boldsymbol{\varepsilon} = \begin{bmatrix} \varepsilon_x \\ \varepsilon_y \\ \varepsilon_z \\ \gamma_{xy} \\ \gamma_{yz} \\ \gamma_{zx} \end{bmatrix} = \mathbf{B}\mathbf{u} \quad (A.3)$$

\mathbf{B} is the strain displacement matrix, while \mathbf{u} is the displacement vector for each node in the element.

$B = [B_1 | B_2 | \dots | B_8]$ such that

$$B_i = \begin{bmatrix} \frac{dN_i}{dx} & 0 & 0 \\ 0 & \frac{dN_i}{dy} & 0 \\ 0 & 0 & \frac{dN_i}{dz} \\ \frac{dN_i}{dy} & \frac{dN_i}{dx} & 0 \\ 0 & \frac{dN_i}{dz} & \frac{dN_i}{dy} \\ \frac{dN_i}{dz} & 0 & \frac{dN_i}{dx} \end{bmatrix} \quad (\text{A.4})$$

To find the derivatives with respect to the global coordinate the inverse of the Jacobian (J) matrix is used as shown:

$$J = \begin{bmatrix} \frac{dN_i}{dr} x_i & \frac{dN_i}{dr} y_i & \frac{dN_i}{dr} z_i \\ \frac{dN_i}{ds} x_i & \frac{dN_i}{ds} y_i & \frac{dN_i}{ds} z_i \\ \frac{dN_i}{dt} x_i & \frac{dN_i}{dt} y_i & \frac{dN_i}{dt} z_i \end{bmatrix} \quad (\text{A.5})$$

$$\begin{pmatrix} \frac{dN_i}{dx} \\ \frac{dN_i}{dy} \\ \frac{dN_i}{dz} \end{pmatrix} = J^{-1} \begin{pmatrix} \frac{dN_i}{dr} \\ \frac{dN_i}{ds} \\ \frac{dN_i}{dt} \end{pmatrix} \quad (\text{A.6})$$

The stress can now be calculated using Hooke's law where, $\sigma = D\varepsilon$, where D is the elasticity matrix, E is the modulus of elasticity, and ν is the Poisson's ratio.

$$D = \frac{E}{(1+\nu)(1-2\nu)} \begin{bmatrix} 1-\nu & \nu & \nu & 0 & 0 & 0 \\ \nu & 1-\nu & \nu & 0 & 0 & 0 \\ \nu & \nu & 1-\nu & 0 & 0 & 0 \\ 0 & 0 & 0 & \frac{1}{2}-\nu & 0 & 0 \\ 0 & 0 & 0 & 0 & \frac{1}{2}-\nu & 0 \\ 0 & 0 & 0 & 0 & 0 & \frac{1}{2}-\nu \end{bmatrix} \quad (\text{A.7})$$

The last point that needs to be covered is Gaussian Integration, a method used to calculate element values for various functions. It approximates the integral by forming a summation consisting of weighted integration points within the element. For 2x2x2 used there are eight integration points where each value equals a combination of $r, s, t = \pm 1/\sqrt{3}$ in the natural element coordinate system. The weighting factor for each point is $w_k = w_l = w_m = 1$.

A defined function can now be defined as follows:

$$f^{(e)} = \int_{-1}^1 \int_{-1}^1 \int_{-1}^1 F(r, s, t) \det J dr ds dt \quad (\text{A.8})$$

$$f^{(e)} \approx \sum_{k=1}^2 \sum_{l=1}^2 \sum_{m=1}^2 w_k w_l w_m F(r, s, t) \det J$$

Finally, it should be noted that the differential volume of the element is equal to

$$dV = \det J dr ds dt \quad (\text{A.9})$$